U-Pb dating of sub-ng/gng g^{-1} U garnet by LA-MC-ICP-MS

Aratz Beranoaguirre[1,2], Leo J. Millonig[1,2], Richard Albert[1,2], Horst R. Marschall[1,2], and Axel Gerdes[1,2]

[1]Frankfurt Isotope and Element Research Center (FIERCE), Goethe-University Frankfurt, 60438 Frankfurt am Main, Germany
[2]Goethe-University Frankfurt, Department of Geosciences, 60438 Frankfurt am Main, Germany

Correspondence to: Aratz Beranoaguirre (beranoaguirre@fierce.uni-frankfurt.de)

Formatted: Superscript

Abstract. Advances in laser ablation inductively coupled plasma mass spectrometry (LA-ICP--MS) have largely focused on improving spatial resolution through progressively smaller laser spot sizes. Here, we explore the opposite end of the analytical limits by investigating the lower concentration limits of in-situ U–Pb geochronology in garnet. Using a Neptune Plus multi-collector ICP-MS equipped with seven ion counters, we developed an analytical workflow specifically designed for metamorphic garnet with ultra-low U concentrations (< 10 ng g^{-1}). The method was used to date garnet from a wide range of ages and geological settings, including granulites, eclogites and hydrothermal demantoids. Uranium concentrations were exceptionally low, even below 1 ng/gng g^{-1} in some cases. At these concentrations, the total amount of uranium U ablated during a single analysis is at femtogram levels, more than three orders of magnitude lower than that of a typical in-situ analysis of zircon. Despite these extremely low signal intensities, geologically meaningful ages were obtained for the analysed samples. Analytical precision depends on the U and radiogenic Pb concentrations, but we have obtained precisions of ca. 5-6 % for garnet containing less than 1 ng/gng g^{-1} U. In garnet with higher U concentrations or ages as old as the Archean, internal precision of ca. 1 % may be achieved. These results expand the applicability of in-situ garnet U-Pb geochronology to the vast majority of metamorphic garnet, providing a powerful new tool for constraining garnet growth, prograde metamorphism, and deep crustal evolution.

Formatted: Superscript

Formatted: Superscript

1 Introduction

The combination of laser ablation (LA) systems with inductively coupled plasma mass spectrometers (ICP-MS) during the 1980s revolutionised in-situ chemical analysis during the 1980s (Gray, 1985; Arrowsmith, 1987). Since the pioneering works, LA-ICP-MS U–Pb geochronology of high-U accessory minerals such as zircon, monazite, or titanite has become a routine analytical tool (e.g., Fryer et al., 1993; Machado and Gauthier, 1996; Willigers et al., 2002; Kosler and Sylvester, 2003; Horstwood et al., 2016). Besides, over the last decade, these analytical capabilities have also been expanded to minerals with lower uranium U concentrations (<10 μg/gμg g^{-1}), including carbonate (Roberts and Walker, 2016; Ring and Gerdes, 2016), sulfate (Beranoaguirre et al., 2022), fluorite (Piccione et al., 2019), and garnet (Seman et al., 2017; Millonig et al., 2020; O'Sullivan et al., 2023), among others. Continuous advances in instrumentation have also been accompanied by progressively smaller laser spot sizes (review in Sylvester and Jackson, 2016), improving the spatial resolution and enabling the distinction of multiple domains within a single crystal (e.g., Chew et al., 2017). In turn, analysing low-U minerals requires a different strategy, in which the main challenge is no longer spatial resolution, but concentration sensitivity. This issue is

Formatted: Superscript

particularly challenging for metamorphic garnet, since its U and Pb amounts are extremely low (Deng et al., 2022). Therefore, being capable of developing a robust analytical strategy for analysing metamorphic garnet would represent a major advance in metamorphic petrology.

Unlike many geochronological systems that either record cooling and exhumation histories (e.g., apatite fission-track, (U–Th)/He, and Ar-based systems) or preferentially date high-temperature metamorphic events (e.g., zircon, monazite, and titanite U–Pb geochronology) (Dodson, 1973; McDougall and Harrison, 1999; Rubatto, 2002; Reiners et al., 2005; Flowers et al., 2009; Kohn et al., 2017), garnet can preserve prograde metamorphic growth histories over a wide range of pressure–temperature conditions (Spear and Parrish, 1996; Caddick and Kohn, 2013), in part due to its exceptionally high closure temperature for the U–Pb system (potentially exceeding 1000 °C; Dahl, 1997; Shu et al., 2024). Traditionally, garnet has been dated by Sm–Nd and Lu–Hf (e.g. Duchêne et al., 1997; Baxter et al., 2017). Although a very high precision can be achieved through these systems, they require laborious mineral separation and dissolution procedures. More recently, the use of tandem mass spectrometry (ICP-MS/MS) has also enabled the in-situ Lu-Hf garnet dating (Simpson et al., 2021). However, the application of in-situ Lu–Hf geochronology remains largely restricted to relatively old metamorphic systems (Caledonian or older; Tamblyn et al., 2022; Kirkland et al., 2025). This limitation may arise from the low radiogenic growth of ^{176}Hf in younger garnet, which hampers analytical precision and age resolution in younger orogens. In contrast, U-Pb garnet geochronology has been used to resolve younger metamorphic events (Peillod et al., 2024; Manzotti et al., 2025). Consequently, U-Pb garnet geochronology (eventually complemented with in-situ Lu-Hf dating) offers a unique opportunity to directly constrain the timing of prograde metamorphism and deep crustal processes.

In this study, we investigate the lower limits of the ~~uranium~~ U and ~~lead~~ Pb concentrations in garnet required to obtain meaningful garnet U-Pb dates by LA-MC-~~ICPMS~~ICP-MS. For that purpose, we have optimised the LA-MC-~~ICPMS~~ICP-MS method on a series of natural, low-U metamorphic garnet specimens from granulites, eclogites, and one gemstone-quality grossular-andradite (i.e. demantoid). The possibility to date garnet crystals with extremely low U concentrations (<1 ~~ng/g~~ng g^{-1}) by LA-MC-~~ICPMS~~ICP-MS is expected to substantially increase the field of application of garnet U-Pb dating, as most of the metamorphic garnet have <50 ~~ng/g~~ng g^{-1} U (Millonig et al., 2020; O'Sullivan et al., 2023; Bartoli et al., 2024; Shu et al., 2024).

Formatted: Superscript

Formatted: Superscript

2 Methodology

U-Pb data were acquired *in-situ* from polished garnet grain mounts and thin sections using a RESOLution 193 nm ArF excimer laser (CompexPro 102) equipped with a two-volume ablation cell (Laurin Technic S155) coupled to a multi-collector (MC)-~~ICPMS~~ICP-MS (Neptune Plus, ThermoScientific) at the Frankfurt Isotope and Element Research Center (FIERCE), Goethe University Frankfurt. The Neptune Plus at FIERCE is equipped with ten Faraday cups and seven ion counters, of which two are classical discrete dynode secondary electron multipliers (SEM) and five compact discrete dynode (CDD) electron multipliers (Fig. 1). This results in two possibilities for the simultaneous detection of the U, Th, and Pb isotopes: I) for moderate U contents of ~ 0.2 to 30 ~~µg/g~~µg g^{-1}, ^{238}U and ^{232}Th are detected on the Faraday cups with 10^{13} Ω amplifiers, ^{207}Pb, ^{206}Pb on the SEM and ^{208}Pb on a CDD (method described in Beranoaguirre et al., 2022); while II) at low U of < 0.2 ~~µg/g~~µg g^{-1}, ^{238}U and, if necessary ^{232}Th, can be measured on the CDD attached to the Faraday cups (H4 and H3, respectively). A summary report of the U-Pb dating procedure is presented in the supplementary material (Table S1), and the analytical results are presented in supplementary Tables S2 to S6.

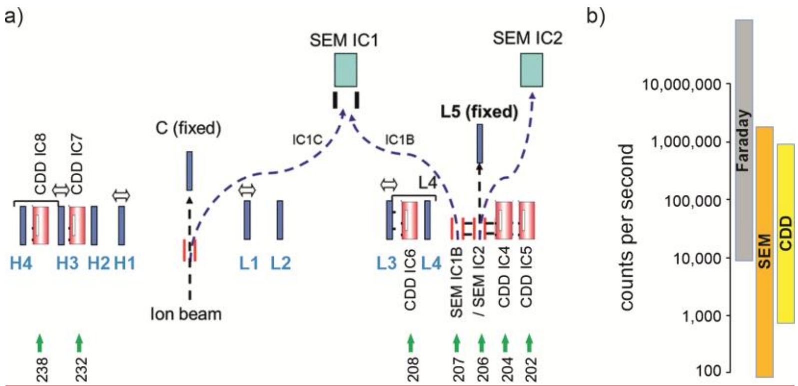

Figure 1. a) Schematic detector configuration of the Neptune Plus MC-ICP-MS used in this study, showing the positions and measured isotopes for the low-U analytical configuration (modified after Richter et al., 2016). b) Approximate signal intensity ranges covered by Faraday cups, secondary electron multipliers (SEM), and compact discrete dynode (CDD) ion counters.

Ablation was performed in a He atmosphere (0.3 l~~/~~ min^{-1}) and mixed in the ablation funnel with daily tuned 0.95 ~~1~~ 1 l ~~/~~min^{-1} Ar and 5–10 ml~~/~~ min^{-1} N_2. Signal strength at the MC-~~ICPMS~~ICP-MS was tuned for maximum sensitivity while keeping oxide formation below 0.5 % (UO/U) and element fractionation low (e.g. Th/U ~ 0.9). This was done by line ablating the SRMNIST 614 glass (Jochum et al., 2011) using a 50 µm spot size, 6 Hz, *ca.* 3.5 J~~/~~ cm^{-2} fluence and a 3 µm~~/~~ s^{-1} line speed. The average sensitivity obtained with this setup was *ca.* 250,000 cps per ~~µg/g~~µg g^{-1} for ^{238}U in the best of the cases. The laser parameters used for instrument tuning are independent of those employed during the analytical sessions, as the purpose of the tuning procedure is solely to optimise ICP-MS operating conditions under a stable signal rather than to reproduce the analytical ablation conditions. The garnet samples were ablated using a round spot size of 193 µm and a fluence of *ca.* 2 J~~/~~ cm^{-2} at 15 Hz. This yielded a depth penetration of *ca.* 0.8 µm~~/~~ s^{-1}. Each analysis consisted of 16 s of background acquisition followed by 18 s of sample ablation and 20 s of washout. The analyses were done in the static mode, measuring ^{206}Pb and ^{207}Pb with SEMs, and ^{202}Hg, ^{204}Pb, (^{208}Pb) and ^{238}U with the CDD and an integration time of 0.131 s (due to electronic issues with the ion counter, ^{208}Pb was not measured in all the sessions).

Formatted: Centered

Formatted: Font: 9 pt, Bold

Formatted: Indent: First line: 0"

Formatted: Font: 9 pt, Bold

Formatted: Superscript

Formatted: Superscript

In each analytical session, soda-lime glass SRMNIST 614 was used as the primary reference material to correct for mass bias (^{207}Pb/^{206}Pb), inter-element fractionation and instrumental drift (^{206}Pb/^{238}U). For this purpose, a block of reference materials was analysed every 50 analyses ~~throughout the analytical sessions~~. A low-U yellow garnet from the Mali Grandite locality (Seman et al., 2017) was used as the matrix-matched reference material to determine the difference in the Pb/U fractionation between garnet and the synthetic glass matrix. This crystal is distinct from the published Mali Grandite reference materials and was selected because its U concentration (ca. 15-20 ng g^{-1}) is sufficiently low to avoid saturation of the ion counters, which occurs at approximately 1,000,000 cps (Fig. 1b). Further details are provided below.~~Mali garnet (Seman et al., 2017) was used as a matrix-matched reference material to determine the difference in the Pb/U fractionation between garnet and the synthetic glass matrix. As the CDDs saturate at around 1,000,000 cps, we have used a low uranium (*ca.* 20 ng/g) yellow-coloured Mali garnet from our collection (see below). Secondary reference garnet materials,~~ Lake Jaco garnet (34.0 ± 1.4 Ma, Seman et al., 2017), together with an in-house quality-control garnet from Balochistan (ID-TIMS age of ca. 45.5 Ma; M. Stifeeva, unpublished data), were analysed to monitor the reproducibility of the analytical procedure.~~and an in-house garnet from Balochistan (TIMS age of ca. 45.5 Ma, Maria Stifeeva, pers. comm.) were measured for quality control.~~ Due to the possible saturation of the ion counters, the secondary garnet crystals were pre-screened to identify domains with sufficiently low-U concentrations (< 1 µg g^{-1}). Those domains also show lower Pb content, and therefore, the ^{207}Pb/^{206}Pb and ^{206}Pb/^{238}U ratios are not affected.

Raw data were corrected offline using an in-house VBA spreadsheet program (Gerdes and Zeh, 2006, 2009). Following background and interference corrections, outliers were rejected based on the time-resolved ^{207}Pb/^{206}Pb and ^{238}U/^{206}Pb ratios, while the Pb and U signals were used to identify and reject data derived from the co-ablation of mineral inclusions or zones with clearly distinct common-Pb and U concentrations compared to the pure garnet. Likewise, outliers in U and/or Pb content were rejected for age calculations, assuming that those analyses reflect inclusions (Fig. ~~1~~2). Data are displayed in Tera-Wasserburg plots (Tera and Wasserburg, 1972), and U-Pb dates were calculated as lower Concordia-curve intercepts using the same algorithms as Isoplot 4.15 (Ludwig, 2012). Age uncertainties shown in the Tera-Wasserburg plots are the within-session uncertainty, considering the within-run precision, counting statistic uncertainties of each isotope, and the excess of scatter and of variance (Horstwood et al., 2016), calculated from the SRMNIST 614 and the Mali garnet, and the expanded uncertainty, which includes the long-term variance of our in-house quality control garnet crystals (2%). All uncertainties are reported at the 2σ level.

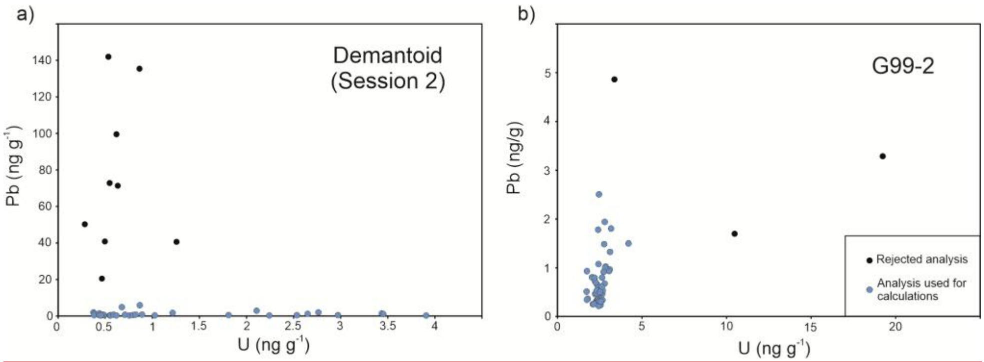

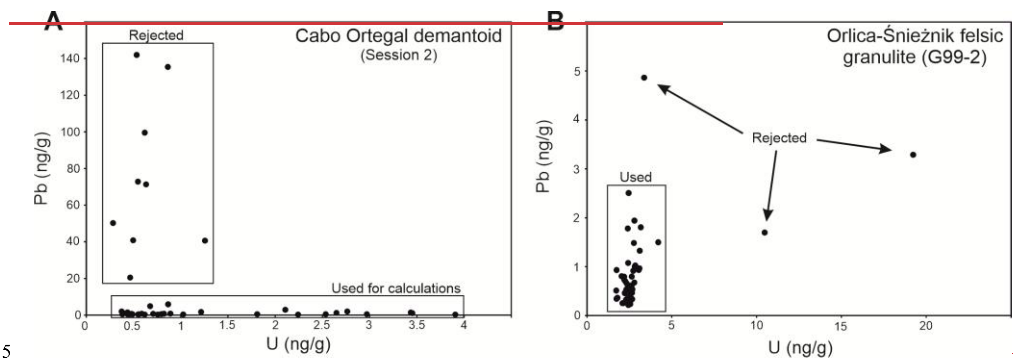

Figure ~~1~~2. Plots of U vs Pb concentration (~~ng/g~~ng g^{-1}), showing the analyses rejected and considered for the age calculations. A) Cabo Ortegal demantoid (session 2) and B) garnet G99-2 from Orlica-Śnieżnik felsic granulite. **Analytical uncertainties are smaller than the plotting symbols and are therefore not visible. Nevertheless, their inclusion would not alter the interpretation of the figure.**

Matrix-matched reference materials (RMs) are an important component of any LA-~~ICPMS~~ICP-MS method (e.g. Schaltegger et al., 2015). With respect to garnet, only a few well-characterised RMs are available to the LA-~~ICPMS~~ICP-MS community in sufficient quantities, although many research groups have developed new RMs over the last few years (e.g. Stifeeva et al., 2019, Salnikova et al., 2019, 2026; Li et al., 2022; Aysal et al., 2023; Beno et al., 2024, Yang et al., 2025). The most popular garnet RMs for U–Pb dating are still the ones published by Seman et al. (2017); the red and yellow varieties of Mali Grandite (LA-~~ICPMS~~ICP-MS U-Pb: 202 ± 2 Ma; ID-TIMS U-Pb: 202.0 ± 1.2 Ma) and the Lake Jaco Grossular (LA-~~ICPMS~~ICP-MS U-Pb: 35 ± 2 Ma; (U-Th)/He: 35 ± 5 Ma). However, U concentrations of >2 ~~µg/g~~µg g^{-1} of the aforementioned garnet RMs would saturate the ion counters, and thus, they are not usable for the method applied in this study. To overcome this issue, we investigated several low-U (<0.5 ~~µg/g~~µg g^{-1}) garnet from the same localities investigated by Seman et al. (2017), and we identified a yellow garnet from the Mali Grandite locality with an average U concentration of 15-20 ng g^{-1}, we found a yellow Mali Grandite with an average U content of 15 ng/g, which was subsequently used as the matrix-matched RM. The secondary reference materials, used for quality control, were compositionally and optically diverse grossular garnet crystals from Lake Jaco, and a dark brown grandite from Balochistan. When assuming the published age of 202 Ma for the yellow Mali, we obtained internally consistent results across multiple sequences for the secondary garnet RMs and different samples. Although no independent age estimates (i.e. TIMS ages) are available for our matrix-match and quality control RMs we consider the obtained U-Pb ages as accurate within their analytical uncertainties, based on the facts that (1) the U-Pb ages for the various Lake Jaco garnet crystals are within the uncertainty of the published ages from that locality (Seman et al., 2017), and (2) the U-Pb age of 384 ± 12 Ma for garnet from sample G99-2 is similar to a Lu-Hf age of 387 ± 5 Ma from that sample (Anczkiewicz et al., 2007; section 3.2). However, we will (re-)calibrate these low-U garnet crystals against well-characterised low-U garnet RMs, once they become available. Furthermore, this potential age ambiguity does not affect the purpose of this contribution.

3 Samples and results

3.1 Cabo Ortegal demantoid (Cabo Ortegal Complex, NW Iberian Massif)

The Cabo Ortegal Complex represents an allochthonous assemblage of continental- and oceanic-derived lithologies that record subduction-related metamorphism prior to their emplacement onto the Gondwanan margin during the Variscan orogeny (e.g. Martínez Catalán et al., 2019). Previous geochronological studies of the complex suggest that the magmatic protoliths (520-460 Ma) were metamorphosed during the Variscan at *ca.* 400-390 Ma followed by a rapid decompression to shallow crustal levels (Beranoaguirre et al., 2020). The demantoid andraditic garnet analysed here was described in detail by Madon et al. (1991). It occurs associated with chlorite and serpentine in fissures cutting across the foliation of the pyroxenite. Due to these cutting relationships, it is believed that the demantoid-bearing veins postdate even the youngest regional granitoids (ca. 280 Ma; Rodríguez et al., 2007).

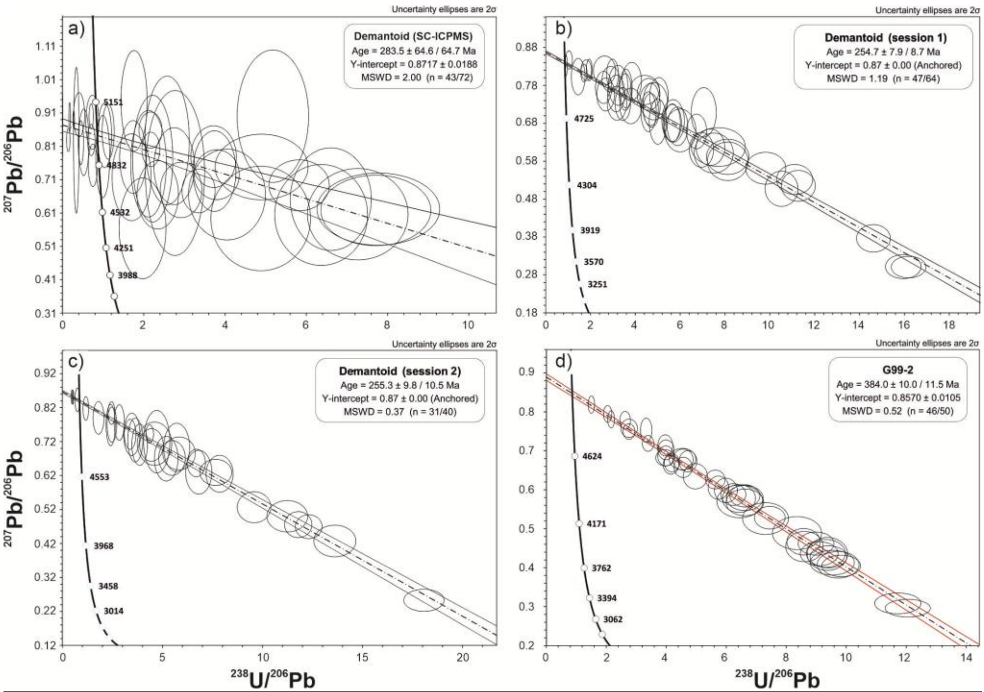
Uncertainty ellipses are 2σ
a)
Demantoid (SC-ICPMS)
Age = 283.5 ± 64.6 / 64.7 Ma
Y-intercept = 0.8717 ± 0.0188
MSWD = 2.00 (n = 43/72)
b)
Demantoid (session 1)
Age = 254.7 ± 7.9 / 8.7 Ma
Y-intercept = 0.87 ± 0.00 (Anchored)
MSWD = 1.19 (n = 47/64)
c)
Demantoid (session 2)
Age = 255.3 ± 9.8 / 10.5 Ma
Y-intercept = 0.87 ± 0.00 (Anchored)
MSWD = 0.37 (n = 31/40)
d)
G99-2
Age = 384.0 ± 10.0 / 11.5 Ma
Y-intercept = 0.8570 ± 0.0105
MSWD = 0.52 (n = 46/50)
207Pb/206Pb
238U/206Pb

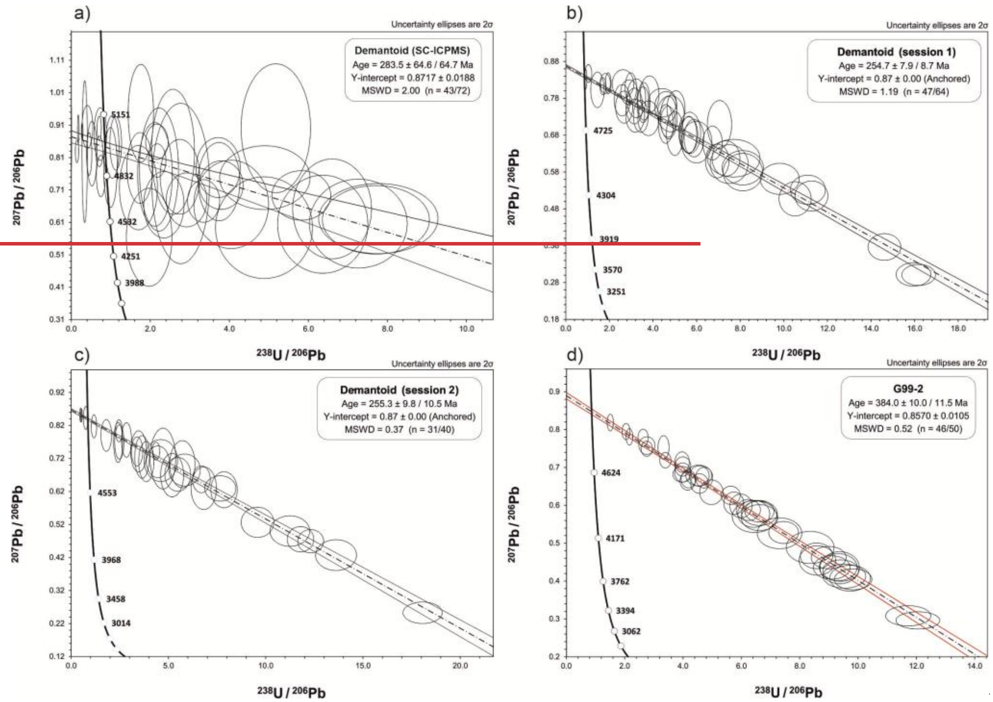

Figure 23. Tera-Wasserburg diagrams of garnet U-Pb analyses for Cabo Ortegal Demantoiddemantoid, analysed with the ElementXR single-collector ICPMSICP-MS (a) and Neptune multi-collectorMC- ICPMSICP-MS (b and c), and sample G99-2 from Orlica-Śnieżnik granuliteBohemian massif (d).

The first attempt to date the demantoid garnet (crystals was made using a single-collector ICPMSICP-MS (the method is described in Millonig et al., 2020 and Beranoaguirre et al., 2022). The resulting data defined a regression line with a lower intercept at 284 ± 65 Ma (MSWD = 2, Fig. 2a3a), and only 43 out of 72 analytical spots had U or Pb concentrations above the detection limits. Subsequently, two sessions were performed with the MC-ICPMSICP-MS. The resulting lower intercept dates for the sessions were 254.7 ± 7.9/8.7 Ma (MSWD = 1.19, n = 47/64, Fig. 2b3b) and 255.3 ± 9.8/10.5 Ma (MSWD = 0.37, n = 31/40, Fig. 2c3c). The regression lines were anchored to a $^{207}Pb/^{206}Pb$ ratio of 0.870 ± 0.005, derived from the mean of the unanchored upper intercept of both sessions,. providing a consistent baseline for comparison. Most of the analyses have extremely low U concentrations between 0.5 and 1 ng/gng g^{-1}, with rare exceptions up to 4 ng/gng g^{-1} (Fig. 1a 2a and 34; Tables S2 and S3).

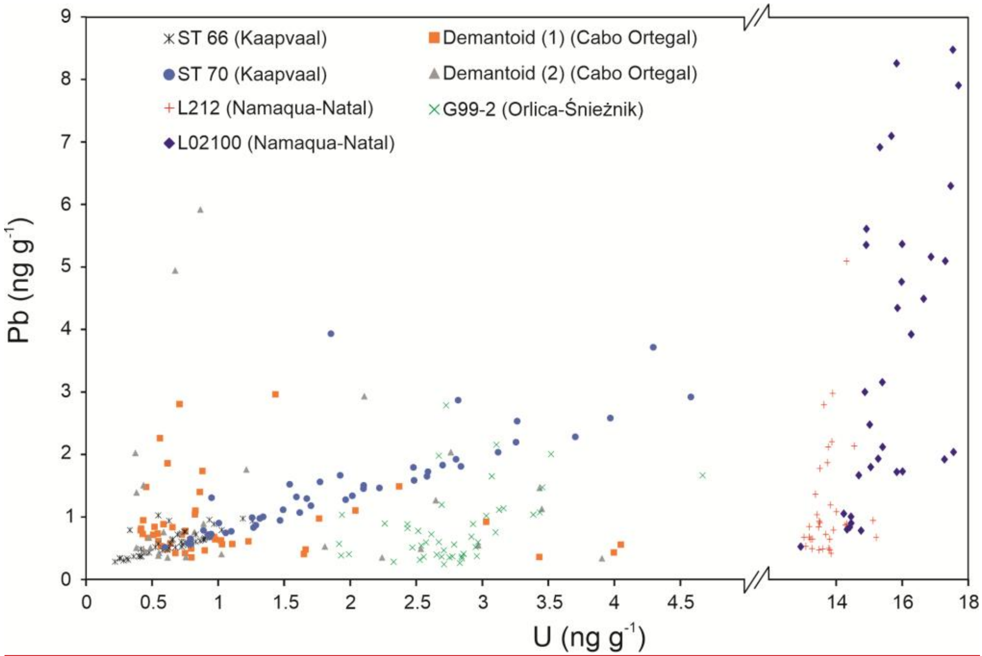
ST 66 (Kaapvaal)
Demantoid (1) (Cabo Ortegal)
ST 70 (Kaapvaal)
Demantoid (2) (Cabo Ortegal)
L212 (Namaqua-Natal)
G99-2 (Orlica-Śnieżnik)
L02100 (Namaqua-Natal)
Pb (ng g-1)
U (ng g-1)
0
1
2
3
4
5
6
7
8
9
0.5
1.5
2.5
3.5
4.5
14
16
18

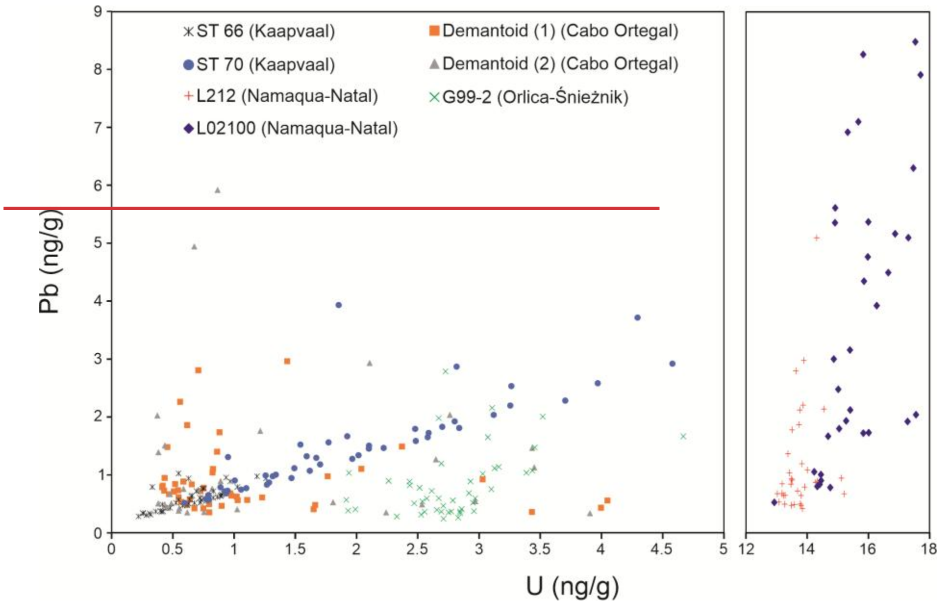

Figure ~~3~~4. Plot of U vs Pb concentration (~~ng/g~~ng g^{-1}) for all the analysed garnet. The rejected analyses (Fig. ~~1~~2) are not considered, to avoid scaling issues. Note the difference ~~on~~ in the x-axis scale for the samples L212 and L02100. In the Kaapvaal samples, ^{208}Pb was not measured and therefore, the Pb concentration is the sum of ^{204}Pb+^{206}Pb+^{207}Pb. Note the discontinuity in the x-axis between 5 and 12 ng g^{-1}. Analytical uncertainties are smaller than the plotting symbols and are therefore not visible.

Formatted: Font: 10 pt

Formatted: Normal

3.2 Orlica-Śnieżnik felsic granulite (NE Bohemian Massif)

The Orlica-Śnieżnik Dome is located on the northeastern margin of the Bohemian Massif in SW Poland. It comprises predominantly amphibolite-facies, partly migmatised, orthogneisses, hosting numerous inclusions of (ultra) high-pressure rocks (e.g. Walczak et al., 2017). Their granitic precursors intruded supracrustal sedimentary successions of Neoprote~~o~~rozoic to Ordovician age and were subsequently metamorphosed during the Variscan orogeny (Szczepański and Ilnicki, 2014).

The garnet analysed here corresponds to the felsic granulite G99-2 studied in detail by Anczkiewicz et al. (2007), who obtained garnet Lu-Hf and Sm-Nd ages of 387 ± 5 Ma and 320 ± 3 Ma, respectively. From the U-Pb analyses performed in our laboratory, an unanchored lower intercept age of 384.0 ± 10.0/11.5 Ma (MSDW = 0.52, n = 46, Fig. ~~2d~~3d) was calculated. The U and Pb contents are homogeneous, varying between 2 and 4 ~~ng/g~~ng g^{-1}, and between 0.3 and 3 ~~ng/g~~ng g^{-1}, respectively (Fig. ~~1b~~ 2b and ~~3~~4; Table S4).

3.3 Granulite xenoliths from the Star kimberlite (Kaapvaal craton, South Africa)

Ultrahigh temperature (UHT) metamorphic crustal granulite xenoliths were found in four kimberlite diatremes from along the central axis of the Witwatersrand basin in the central Kaapvaal craton (Schmitz and Bowring, 2003). The xenoliths are K-free, Mg-Al-rich UHT granulites with abundant garnet, sillimanite, rutile, graphite and sulphides, and local occurrence of sapphirine, orthopyroxene, plagioclase and quartz. Metamorphic conditions have been estimated at temperatures above 1050°C and pressures between 0.9–1.2 GPa (Dawson et al., 1997). Zircon and monazite gave U–Pb ages of approximately 2.7 Ga (Schmitz and Bowring, 2003). The xenoliths were brought to the surface by Cretaceous kimberlite magmatism at approximately 120 Ma.

The results of these samples have already been published and discussed in detail by Shu et al. (2024). The analyses of the garnet ~~of~~ in that ~~work~~ publication followed the method described here, and considering that the aim of this work is purely methodological, two examples of those rocks are shown: the one with the lowest U concentration (sample ST66) and the one with the highest precision (ST 70). The latter was achieved by anchoring the regression line to a sillimanite crystal analysis, assuming that both minerals are in equilibrium. ~~.~~The samples ST66 and ST70 define regression lines with lower intercepts at 3096 ± 63/70 Ma (MSWD = 2.18, n = 53/53, Fig. ~~4a~~5a) and 3096 ± 37/48 Ma (MSWD = 3.05, n = 53/58, Fig. ~~4b~~5b). As stated above, sample ST66 shows the lowest U content among the samples presented in this work, varying from 0.3 to 2.2 ~~ng/g~~ng g^{-1}, whereas sample ST70 has a more variable U content, between 1 and 17 ~~ng/g~~ng g^{-1}. Pb and U contents are positively correlated. Unfortunately, it was not possible to measure the ^{208}Pb isotope, so the calculated Pb content is the sum of ^{204}Pb+^{206}Pb+^{207}Pb. The resulting Pb concentrations do not exceed 1 ~~ng/g~~ng g^{-1} for sample ST66 and 6 ~~ng/g~~ng g^{-1} for sample ST70, except in two spots (Fig. ~~3~~4; Table S5).

3.4 Eclogite xenoliths from the Namaqua-Natal Belt (South Africa)

Multiple Cretaceous kimberlite pipes occurring on the Proterozoic Namaqua-Natal-~~Natal~~ Fold Belt, which surrounds the Archean Kaapvaal craton, have brought to the surface a significant amount of high-pressure eclogite, granulite and pyroxenite xenoliths (Le Roex et al., 2020). The eclogites are mainly bimineralic (garnet-clinopyroxene) with accessory rutile and coesite/quartz (and even diamond), although kyanite-bearing eclogites are also described. As for the Kaapvaal craton granulites, we have analysed several samples from different kimberlites of the area, but only two of them are discussed in the present manuscript. Data points from sample L02100 define a regression line with a lower intercept at 102.7 ± 3.6/3.9 Ma (MSWD = 1.05; n = 37/41; Fig. ~~4c~~5c), whereas the analyses of sample L212 define a regression line with a lower intercept at 105.5 ± 2.5/2.9 Ma (MSWD = 0.92; n = 34/48; Fig. ~~4d~~5d). Both samples have relatively homogeneous U contents of 14–16 ~~ng/g~~ng g^{-1} on average. Sample L212 also shows a homogeneous Pb content between 0.5 and ~~4~~ 4 ~~ng/g~~ng g^{-1}, whereas sample L02100 display a higher variability with up to 14 ~~ng/g~~ng g^{-1} (Fig. ~~3~~4, Table S6).

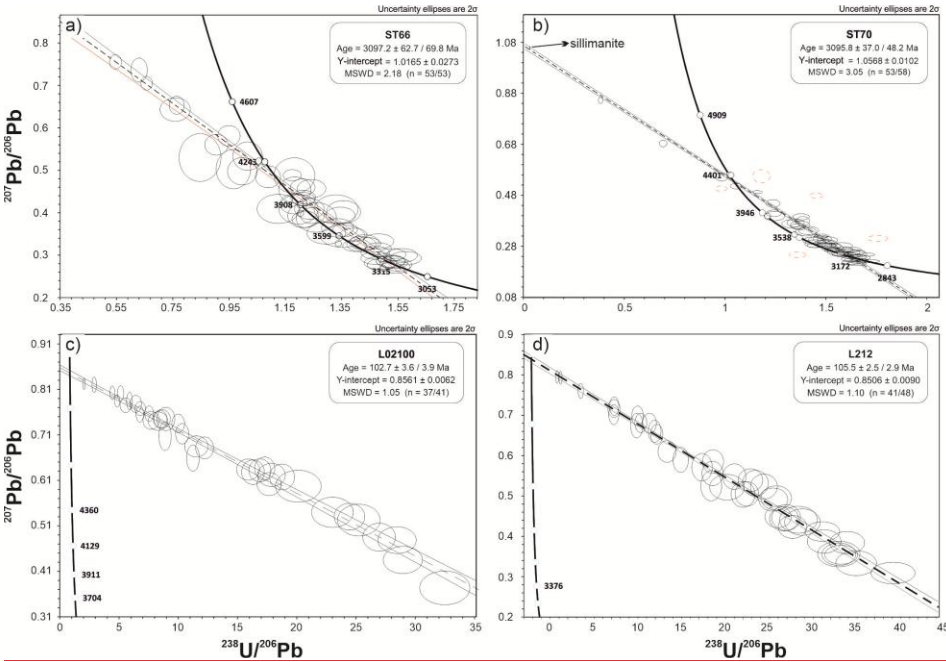
Uncertainty ellipses are 2σ
a)
ST66
Age = 3097.2 ± 62.7 / 69.8 Ma
Y-intercept = 1.0165 ± 0.0273
MSWD = 2.18 (n = 53/53)
4607
4243
3908
3599
3315
3053
Uncertainty ellipses are 2σ
b)
sillimanite
ST70
Age = 3095.8 ± 37.0 / 48.2 Ma
Y-intercept = 1.0568 ± 0.0102
MSWD = 3.05 (n = 53/58)
4909
4401
3946
3538
3172
2843
Uncertainty ellipses are 2σ
c)
L02100
Age = 102.7 ± 3.6 / 3.9 Ma
Y-intercept = 0.8561 ± 0.0062
MSWD = 1.05 (n = 37/41)
4360
4129
3911
3704
Uncertainty ellipses are 2σ
d)
L212
Age = 105.5 ± 2.5 / 2.9 Ma
Y-intercept = 0.8506 ± 0.0090
MSWD = 1.10 (n = 41/48)
3376
207Pb/206Pb
238U/206Pb

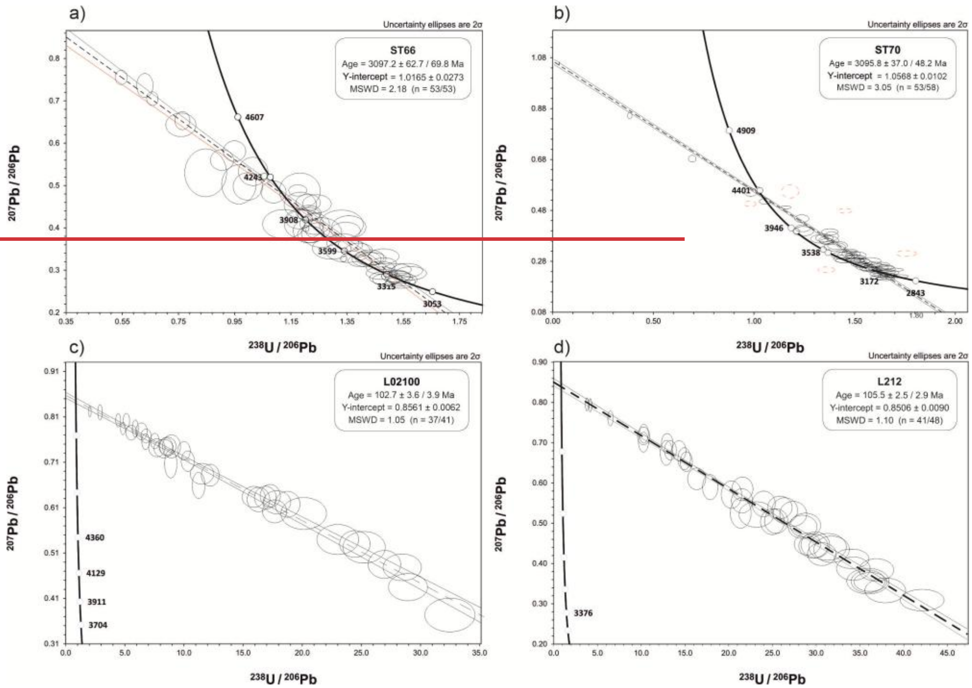

Figure ~~4~~5. Tera-Wasserburg diagrams of garnet U-Pb analyses for the samples from Kaapvaal craton ST66 and ST70 (a and b; Shu et al., 2024)~~)~~ and Namaqua-Natal Belt, L02100 and L212 (c and d), respectively~~)~~.

4 Discussion

4.1 Bulk ~~Uranium~~uranium content: zircon vs. garnet

One of the main strengths of the LA-~~ICPMS~~ICP-MS technique is its ~~good~~ high spatial resolution. In contrast with the bulk dating method (TIMS), the laser ablation method only analyses a ~~tiny~~ relatively small volume of the targeted mineral, and therefore, the bulk amount of U analysed is limited. Besides, not all the ablated material reaches the detector, and the useful yield for U (=ions detected/total number of atoms in sample volume for a species of interest, Schaltegger et al., 2015) is variable depending on the utilised instrument.

In the case of this study, the ablation of garnet with a 193 µm spot size, 15 Hz and ~2 J cm^{-2} for 18 seconds results in a *ca.* 15 µm deep ablation pit. The depth is variable depending on the composition of the garnet, typically between 8–22 µm.

Figure 6 shows a representative ablation pit from sample L02100 together with its measured depth profile, and similar pit depth measurements were routinely performed on all analysed samples to estimate the average ablated volume as accurately as possible. Considering an average pit depth of 15 µm, each analysis corresponds to a total volume of *ca.* 600,000 µm^3 or 2.3 µg of ablated material, assuming a mean garnet density of 3.9 g cm^{-3} (Table 1). Li et al. (2022) recently reported skarn garnet with up to 75 µg g^{-1} U. Applying the above calculations, this corresponds to *ca.* 100 pg U per ablated spot, and *ca.* 8 pg U and 0.4 pg Pb for a Mali garnet analysis (6 µg g^{-1} U and 0.3 µg g^{-1} Pb, Seman et al., 2017). However, the metamorphic garnet rarely exceeds U concentrations of ~100 ng g^{-1} (Deng et al., 2022). For example, a regional metamorphic garnet with 90 ng g^{-1} U (sample SS-1 of Millonig et al., 2020) would yield *ca.* 0.1 pg U per analytical spot. In the present study, sample ST66 has the lowest U concentration, with an average concentration of 1.1 ng g^{-1}. The total U ablated during such a spot analysis is *ca.* 1 fg (femtogram; 10^{-15} g). This is *ca.* 3,500 times less U than for a renowned GJ-1 zircon analysis (287 µg/g U_{avg}; 26 µg/g Pb_{avg}, Jackson et al., 2004), which yields 3.5 pg of U and 0.30 pg of Pb per spot, calculated for a 20 µm spot size, 15 µm pit depth and *ca.* 10 ng of ablated material (considering a zircon density of 4.65 g cm^{-3}) (Table 1). In the case of this study, the ablation of garnet with a 193 µm spot size, 15 Hz and ~2 J/cm² for 18 seconds results in a *ca.* 15 µm deep ablation pit. This corresponds to a total volume of *ca.* 600,000 µm^3 or 2.3 µg of ablated material, assuming a mean garnet density of 3.9 g/cm³ (Table 1). Li et al. (2022) recently reported skarn garnet with up to 75 µg/g U. Applying the above calculations, this corresponds to *ca.* 100 pg U per ablated spot, and *ca.* 8 pg U and 0.4 pg Pb for a Mali garnet (6 µg/g U and 0.3 µg/g Pb, Seman et al., 2017) analysis. However, the metamorphic garnet rarely exceeds U concentrations of ~100 ng/g (Deng et al., 2022). For example, a regional metamorphic garnet with 90 ng/g U (sample SS-1 of Millonig et al., 2020) would yield *ca.* 0.1 pg U per analytical spot. In the present study, sample ST66 has the lowest U concentrations with an average concentration of 1.1 ng/g. The total Uranium ablated during such a spot analysis is *ca.* 1 fg (femtogram; 10^{-15} g). This is *ca.* 3,500 times less U than for a renowned GJ-1 zircon analysis (287 µg/g U_{avg}; 26 µg/g Pb_{avg}, Jackson et al., 2004), which yields 3.5 pg of U and 0.30 pg of Pb per spot, calculated for a 20 µm spot size, 15 µm pit depth and *ca.* 10 ng of ablated material (considering a zircon density of 4.65 g/cm³) (Table 1).

Material / Sample	**U concentration (ng/gng g^{-1})**	**Total U per spot (pg)**
GJ-1 zircon (Jackson et al., 2004)	287,000	3.5
Mali garnet (Seman et al., 2017)	6,000	~8
Skarn garnet (Li et al., 2022)	75,000	~100
Metamorphic garnet SS-1 (Millonig et al., 2020)	90	~0.10
Namaqua–Natal eclogite L212	14	~0.032

Orlica–Śnieżnik granulite (G99-2)	2–4	~0.003–0.009
Cabo Ortegal demantoid	1.3	~~~0.001–~~0.002
Kaapvaal granulite ST66	~~1.1~~0.7	~0.001

Table 1. Comparison of ~~Uranium~~U content analysed in a single LA-ICP-MS spot analysis for different minerals. Total U per spot was calculated from the average U concentration of each material and the corresponding ablated mass. Garnet calculations assume a 193 µm spot diameter, ~15 µm pit depth, a density of 3.9 g cm⁻³, and an ablated mass of ~2.3 µg per analysis. The GJ-1 zircon calculation assumes a 20 µm spot diameter, ~15 µm pit depth, a density of 4.65 g cm⁻³, and an ablated mass of ~0.012 µg. ~~Calculations are done for the regular ablation parameters (see text for further details).~~ The ~~figure~~ table illustrates the extreme reduction in available parent isotope mass when dating low-U metamorphic garnet, with the ST66 granulite ~~and Cabo Ortegal demantoid~~ analyses containing only ~1~~–3~~ fg U per spot, approximately 3,500 times less ~~Uranium~~ U than a typical GJ-1 zircon analysis and up to five orders of magnitude less than high-U skarn garnet.

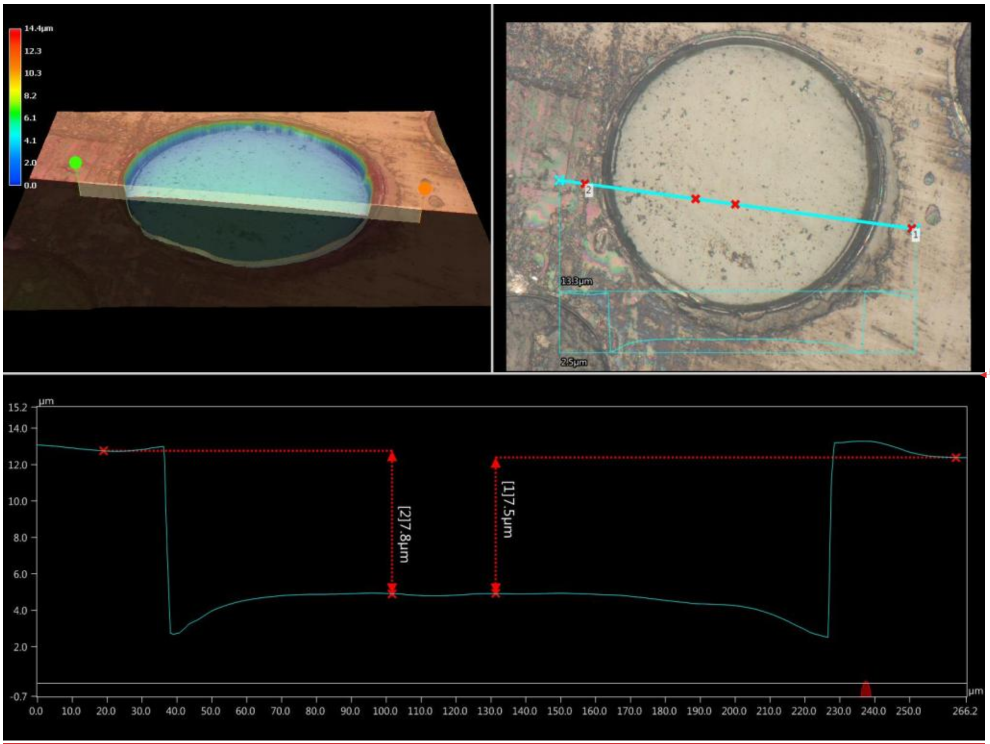

Figure 6. Illustrative example of an LA-ICP-MS ablation pit produced in garnet (sample L02100) using a 193 µm spot size, 15 Hz repetition rate, a fluence of ~2 J cm^{-2}, and an ablation time of 18 s. The image was acquired with a Keyence digital microscope. a) Three-dimensional topographic image of the ablated pit. b) Optical image showing the position of the measured depth profile. c) Corresponding depth profile across the pit. The illustrated pit is approximately 8 µm deep; pit depths measured for different garnet typically range from 8 µm to 22 µm, depending on garnet composition.

Samples with even lower amounts of U could be analysed, if they are older and have higher ^{238}U than ^{206}Pb for the majority of the spots (as well as $^{206}Pb > ^{207}Pb$), with the exception of the high common-Pb analyses. As an example, a 200 Ma old concordant analysis will have *ca.* 30 times more ^{238}U than ^{206}Pb and *ca.* 20 times more ^{206}Pb than ^{207}Pb (or 600 times more ^{238}U than ^{207}Pb). In turn, a 3 Ga sample intercepts the Concordia at *ca.* 1.5 ($^{238}U/^{206}Pb$) and 0.25 ($^{207}Pb/^{206}Pb$), the ^{238}U being only *ca.* 6 times more abundant than ^{207}Pb. Hence, for such old samples, it would be possible to date a garnet with even lower U concentrations.

Formatted: Centered

Formatted: Not Superscript/ Subscript

Formatted: Not Superscript/ Subscript

Formatted: Superscript

Formatted: Not Superscript/ Subscript

Formatted: Not Superscript/ Subscript

Formatted: Not Superscript/ Subscript

Formatted: Not Superscript/ Subscript

4.2 Background level, limit of detection, limit of quantification and analytical precision

Such low U and Pb concentrations in garnet correspond to a few hundred counts per second (cps), and therefore, the background level plays a vital role, especially for ^{207}Pb, the least abundant of the measured isotopes. Background Pb may come from different sources, such as a memory effect in the tubing, contamination/dirt in gas-line connections, the cones or the laser cell. Although careful cleaning of those parts is effective in reducing their Pb contribution, Pb derived from the Ar and He gas supplies is unavoidable. This contribution varies from day to day (Fig. ~~5~~ 7 shows the background level at the FIERCE laboratory observed over one and a half years), and it is a critical factor for the analytical performance. ~~Despite the variations in background intensity between analytical sessions, the background is generally stable within a single session, which allows low limits of detection.~~ Following the approach proposed by Pettke et al. (2012), the limits of detection for average background signals of 10 cps and 400 cps are approximately 6 pg~~/~~ g^{-1} and 30 pg~~/~~ g^{-1}, ~~or 2 to 8 cps,~~ respectively (corresponding to net signals of 2 cps and 8 cps at the detection limit, considering the aforementioned sensitivity of 250,000 cps per ~~μg/g~~μg g^{-1}). Although the background intensity differs by a factor of 40 in these examples, the limit of detection increases by only about a factor of 4-5 because the background count rate enters the calculation under the square root. ~~However~~On the contrary, the limit of quantification (Currie, 1995), defined as 10 times the standard deviation of the measured background signal, drastically increases with increasing background intensity. For example, during low-background sessions, the standard deviation of the ^{207}Pb background can be as good as 5-6 cps, corresponding to a limit of quantification of approximately 50–60 cps (Fig.6). In contrast, during one of the highest-background sessions, the standard deviation is ca. 200 cps, increasing the limit of quantification to 2000 cps. Thus, a high Pb background prevents reliable analysis of low ^{207}Pb samples, as their signal falls below the quantification limit. In practice, samples with ultra-low-U and -Pb garnet are only analysed during sessions in which the ^{207}Pb background remains below 50 cps.

~~However, even though the Pb can be reliably detected, the precision of each analysis is also crucial. Figure 6 shows the relationship between the ^{207}Pb signal intensity and the within-run precision of the ^{207}Pb/^{206}Pb ratio, over several sequences covering a large range of ^{207}Pb concentrations. As could be expected from counting statistics, a lower ^{207}Pb signal results in a lower precision. Analyses yielding ^{207}Pb signals above 2,500 cps commonly achieve uncertainties of less than 1% (2 SE), whereas signals below 2,500 cps typically result in uncertainties above 1% (2 SE). Furthermore, as the signal gets closer to the limit of quantification (≤ 100 cps), there is a strong increase in the uncertainty, which highlights the limit of the technique.~~

~~Another potential source of uncertainty, although it is not considered in our calculations, is the variance of the Uranium decay, or in other words, the statistical uncertainty coming from the decay of a small number of radioactive atoms. In the case of dating high-U minerals, as well as old samples that have been decaying for a long time, such uncertainty can be considered negligible and that is likely why it is not considered in Geochronology. However, physicists studying slow decay processes have discussed this phenomenon (e.g. Opendak and Wildenhain, 1994). In the case of low-U and young minerals (<1 ng/g U or <10 Ma old), this incertitude may be of importance and needs to be considered. Nonetheless, young samples~~

with such a low content of uranium are currently not measurable with the analytical setup discussed in this study, as the amount of radiogenic ^{207}Pb is below the limit of detection.

In addition to the analytical precision of each individual spot measurement, the precision of U-Pb dating for non-concordant minerals like garnet when using a Tera-Wasserburg diagram is also controlled by how accurately the regression line can be defined. This strongly depends on the variability of the ^{238}U/^{206}Pb and ^{207}Pb/^{206}Pb ratios; the larger the spread in these ratios, the smaller will be the uncertainty on the lower intercept of the regression line with the Concordia curve and, thus, the more precise the obtained age will be. The internal precision for the analyses of the Cabo Ortegal demantoid are ± 4.7 % and ± 6.3 % for the absolute garnet ages, even with only 40 analytical spots and an extremely low U concentration (mainly below 1 ng/g, Fig. 3). In turn, U concentrations of 2–4 ng/g, as for the Orlica-Śnieżnik felsic granulite garnet, significantly improve the precision to ca. ± 3 % absolute age uncertainty. Furthermore, the analyses of sample ST70 resulted in an internal age precision of ca. ± 1 %. In this case, two factors concurred to result in such precise data: I) higher U and Pb contents and II) the Archean age of the sample, as older samples benefit the most from the technique due to their more abundant daughter isotopes ^{206}Pb and ^{207}Pb. However, in samples as young as the Cretaceous Namaqua-Natal belt eclogites, we have obtained precisions of ca. ±3 % at U concentrations of ca. 14–16 ng/g. The results obtained for the demantoid in two independent sessions are reproducible within uncertainty. Likewise, the U-Pb age of the garnet from Orlica-Śnieżnik felsic granulite, 384 ± 12 Ma, is in agreement with the Lu-Hf age reported by Anczkiewicz et al. (2007, 387 ± 5 Ma). Thus, the procedure described in this study produces accurate results within the internal precision of the technique.

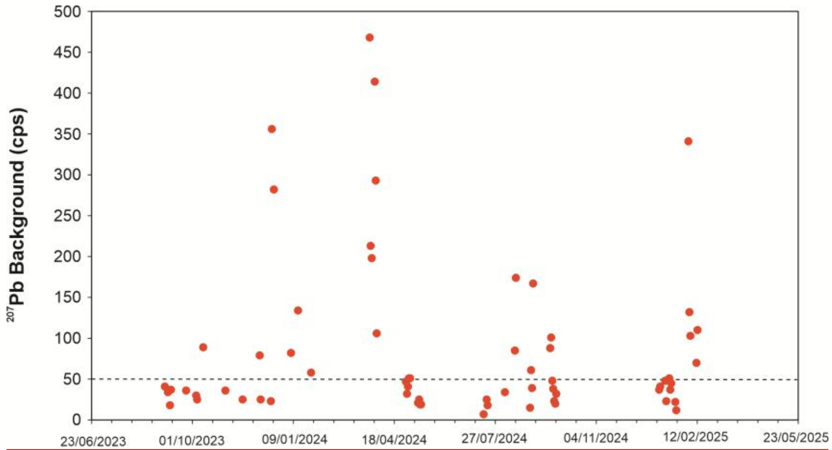

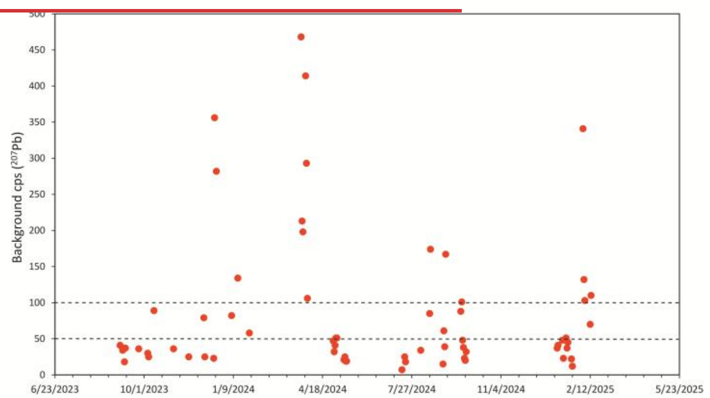

Figure ~~5~~7. ^{207}Pb background (in cps) at the FIERCE laboratory during a period of ca. one and a half years. The spots show the average ^{207}Pb background for each of the days.

However, even though the Pb can be reliably detected, the precision of each analysis is also crucial. Figure 8 shows the relationship between the ^{207}Pb signal intensity and the within-run precision of the ^{207}Pb/^{206}Pb ratio, over several sequences covering a large range of ^{207}Pb concentrations. As could be expected from counting statistics, a lower ^{207}Pb signal results in a lower precision. Analyses yielding ^{207}Pb signals above 2,500 cps commonly achieve uncertainties of less than 1% (2 SE), whereas signals below 2,500 cps typically result in uncertainties above 1% (2 SE). Furthermore, as the signal gets closer to the limit of quantification (≤ 100 cps), there is a strong increase in the uncertainty, which highlights the limit of the technique.

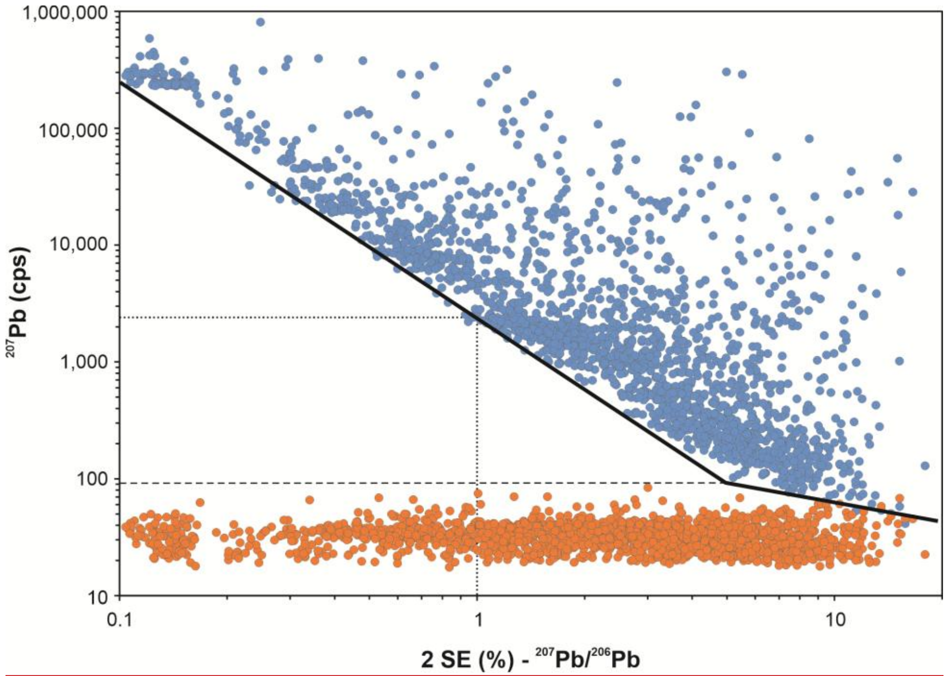

1,000,000
100,000
10,000
1,000
100
10
^{207}Pb (cps)
0.1
1
10
2 SE (%) - ^{207}Pb/^{206}Pb

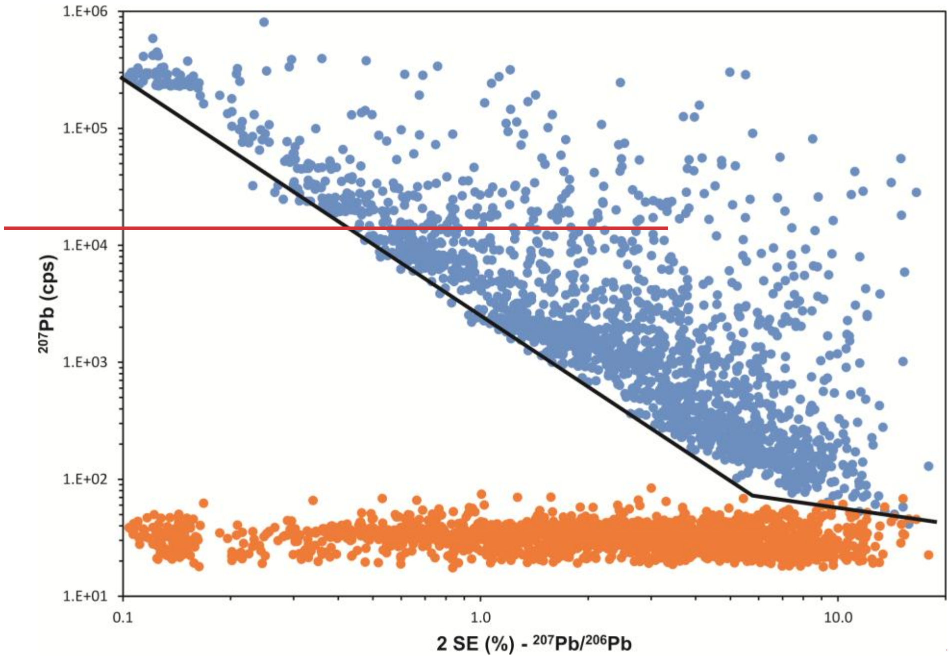

Figure ~~6~~8. ~~^{207}Pb signal intensity (blue symbols) and calculated limit of quantification (orange symbols) plotted against the within-run precision of the ^{207}Pb/^{206}Pb ratio (2SE, %). The limit of quantification was calculated as ten times the standard error of the measured ^{207}Pb background signal, following Currie (1995). The correlation between the ^{207}Pb intensity and the within-run precision is clearly observable.~~Relationship between the ^{207}Pb signal intensity and the within-run precision of the ^{207}Pb/^{206}Pb ratio (2SE, %; blue symbols). Orange symbols indicate the limit of quantification, calculated as ten times the standard deviation of the measured ^{207}Pb background signal (Currie, 1995). The black line represents the minimum achievable within-run precision as a function of the ^{207}Pb signal intensity. The pronounced increase in uncertainty below approximately 100 cps (horizontal dashed line) marks the practical analytical limit of the method. A ^{207}Pb signal of approximately 2500 cps (dotted lines) is typically required to achieve a within-run precision of ~1 % (2SE). Analytical uncertainties are smaller than the plotting symbols and are therefore not visible.

Formatted: Indent: First line: 0"

Another potential source of uncertainty, although it is not considered in our calculations, is the variance of the U decay, or in other words, the statistical uncertainty coming from the decay of a small number of radioactive atoms. In the case of dating high-U minerals, as well as old samples that have been decaying for a long time, such uncertainty can be considered negligible and that is likely why it is not considered in geochronology. However, physicists studying slow decay processes have discussed this phenomenon (e.g. Opendak and Wildenhain, 1994). In the case of low-U and young minerals (<1 ng g^{-1} U or <10 Ma old), this incertitude may be of importance and needs to be considered. Nonetheless, young samples with such a low content of U are currently not measurable with the analytical setup discussed in this study, as the amount of radiogenic ^{207}Pb may be below the limit of quantification.

In addition to the analytical precision of each individual spot measurement, the precision of U-Pb dating for non-concordant minerals like garnet when using a Tera-Wasserburg diagram is also controlled by how accurately the regression line can be defined. This strongly depends on the variability of the ^{238}U/^{206}Pb and ^{207}Pb/^{206}Pb ratios; while samples with high common-Pb contributions tend to cluster near the upper intercept, a larger spread in these ratios yields a smaller uncertainty on the lower intercept with the Concordia curve and, consequently, a more precise age. The internal precision for the analyses of the Cabo Ortegal demantoid are ± 4.7 % and ± 6.3 % for the absolute garnet ages, even with only 40 analytical spots and an extremely low U concentration (mainly below 1 ng g^{-1}, Fig. 4). In turn, U concentrations of 2–4 ng g^{-1}, as for the G99-2 garnet (Orlica-Śnieżnik granulite), significantly improve the precision to ca. ± 3 % absolute age uncertainty. Furthermore, the analyses of sample ST70 resulted in an internal age precision of ca. ± 1 %. In this case, two factors concurred to result in such precise data: I) higher U and Pb contents and II) the Archean age of the sample, as older samples benefit the most from the technique due to their more abundant daughter isotopes ^{206}Pb and ^{207}Pb. However, in samples as young as the Cretaceous Namaqua-Natal belt eclogites, we have obtained precisions of ca. ±3 % at U concentrations of ca. 14–16 ng g^{-1}. The results obtained for the demantoid in two independent sessions are reproducible within uncertainty. Likewise, the U-Pb age of the garnet from G99-2, 384 ± 12 Ma, is in agreement with the Lu-Hf age reported by Anczkiewicz et al. (2007, 387 ± 5 Ma). Thus, the procedure described in this study produces accurate results within the internal precision of the technique.

4.3 Applications of the technique

U-Pb dating of garnet is becoming a relatively common tool, above all for skarn garnet, as they typically contain several µg/gµg g^{-1} of U (e.g., Reinhardt et al., 2022). However, the applicability of the technique is rather limited in metamorphic, typically almandine-pyrope, garnet due to their low U content (Millonig et al., 2020; Cerva-Alves et al., 2021; Schannor et al., 2021; O'Sullivan et al., 2023; Mark et al., 2023; Peillod et al., 2024; Manzotti et al., 2025), and the common presence of high-U mineral inclusions. The method described here allows for the analysis of very low-U garnet, or a reduction in laser spot sizes to avoid inclusions (cf. Walters et al., 2025) and thus has enormous potential to become a routine tool for petro(chrono)logical investigations.

Moreover, due to the high closure temperature of the U-Pb system in garnet (exceeding 1050-1100 ºC; Shu et al., 2024), it appears to be the most reliable method for dating its formation and thus the associated mineral reactions. In many cases, these events cannot be accurately constrained by traditional geochronometers like zircon, apatite, rutile, or monazite due to inherent limitations in such settings. For instance, rutile exhibits relatively low U-Pb closure temperaturesIn many cases,

~~this cannot be determined by traditionally datable minerals such as zircon, rutile, or monazite~~ (<600 °C, depending on grain size; Cherniak, 2000; Zack and Kooijman, 2017). Similarly, minerals like apatite and monazite are prone to fluid-assisted coupled dissolution–reprecipitation or recrystallisation during subsequent hydrothermal events (e.g., Harlov et al., 2002; 2011; Putnis, 2009). Conversely, highly resilient minerals like zircon frequently retain inherited domains that complicate both their geochronological analysis and geological interpretation (e.g., Rubatto, 2017). Furthermore, if such minerals occur as inclusions within garnet, they may remain shielded from fluid interaction, thereby recording pre-metamorphic ages. Finally, many of these accessory phases are scarce or absent in mafic and ultramafic rocks. ~~because of I) their lower closure temperatures (in some contexts/minerals) or II) their tendency to recrystallise (e.g., Rubatto, 2017), in addition to the fact that they rarely occur in mafic rocks.~~ The granulite and eclogite xenoliths from the Kaapvaal craton and Namaqua-Natal belt analysed here are good examples, similar to the peridotitic garnet dated by O'Sullivan et al. (2023). Even though scarce rutile has been found in a few samples, the most common mineral assemblage is formed only by garnet and clinopyroxene. In addition, the low U content and their small grain sizes do not necessarily make metamorphic rutile a better geochronometer. In this work, we have successfully dated garnet from those geological contexts, despite their very low U contents. Larger sample sets of both the Kaapvaal craton granulites and the Namaqua-Natal belt eclogites have been analysed, and the results are reported and discussed in Shu et al. (2024).

Likewise, at present, the only possible way to date the hydrothermal garnet-chlorite-serpentine veins crosscutting the pyroxenites at Cabo Ortegal is by U-Pb dating of the Cabo Ortegal demantoid. The rock is near-monomineralic garnet, and because the associated chlorite lacks K and Rb, traditional K–Ar or Rb–Sr geochronological techniques cannot be applied~~The rock is near-monomineralic garnet, and the associated chlorite lacks K and Rb to date it by means of the K-Ar or Rb-Sr techniques~~. As the garnet occurs in fissures cutting across the foliation of the pyroxenite, and likely the whole complex in depth, ages younger than the plutons of the area were expected (youngest plutons are ca. 280 Ma, Rodriguez et al., 2007). The results of ca. 255 Ma obtained here are similar to the Aia Pluton age in the westernmost Pyrenees (dated to~~at~~ 267 Ma, Denèle et al., 2012). Those authors interpreted the age as reflecting the earliest evidence of an extensive regime that led later to the formation of the Bay of Biscay rift. Thus, the garnet-bearing veins at the Cabo Ortegal Complex may have formed during the same event.

The speed of data acquisition provided by laser-ablation techniques also allows for obtaining a large dataset in a short time (, in contrast to the more precise acid-digestion-based garnet dating methods (Lu-Hf and Sm-Nd; e.g., Münker et al., 2001; Anczkiewicz and Thirlwall, 2003). This gives the opportunity to investigate a larger number of samples, either with a higher sampling density in a given area of investigation, or by extending the investigation to a much larger area. In some cases, a larger dataset can reveal small-scale metamorphic processes that have been hidden due to sampling bias (including samples not analysed due to the appearance of alteration). For instance, the U-Pb age of garnet from the NE Bohemian Massif obtained here is within the uncertainty of the Lu-Hf age of this sample (Anczkiewicz et al., 2007). Walczak et al. (2017) dated other mesocratic and mafic granulites from the same outcrop sampled by Anczkiewicz et al. (2007) using the same analytical protocols. Their results pointed to a younger event of garnet formation at *ca.* 345–340 Ma and they attributed this inconsistency to a contribution of inherited Hf in the whole-rock analysis of Anczkiewicz et al. (2007). The *in-situ* U-Pb dating in garnet circumvents the inherited Hf issue as potential inclusions can be avoided by direct petrographic observations (i.e. setting spots in clean domains) or rejecting analysis with distinct U and/or Pb content (Fig. 12). In any case, the fact that the sample analysed by Walczak et al. (2017) is not exactly the same, may indicate that the geological evolution of the area is more complex (polymetamorphic?) than previously thought.

5 Conclusions

This study demonstrates that meaningful U–Pb ages can be obtained by LA-MC-ICP-MS from garnet containing U concentrations lower than 1 ng/gng g^{-1}. The analysis of all Pb and U isotopes using ion counters, combined with high-sensitivity analytical conditions, permits reliable regression lines to be defined in Tera–Wasserburg space, even for minerals that contain up to 300,0500 times less U than commonly analysed accessory minerals such as the GJ1 reference zircon.

The method yields reproducible and geologically meaningful ages across a wide range of sample ages and compositions. Independent analytical sessions on the Cabo Ortegal demantoid produced indistinguishable ages within uncertainty, while the age obtained for the Orlica–Śnieżnik granulite garnet agrees with previously published Lu–Hf data. The precision achieved depends on the U and Pb concentrations, with internal uncertainties of ca. ±5–6 % for garnet containing <1 ng/gng g^{-1} U and ca. ±3 % for samples with higher U contents (2–4 ng/gng g^{-1}). Moreover, in Archean samples, uncertainties as low as ±1 % were achieved, as older samples benefit from their higher radiogenic Pb contents.

These results significantly expand the applicability of in-situ garnet U–Pb geochronology. As most of the metamorphic garnet contain only a few ng/gng g^{-1} U or less, this analytical approach opens the possibility of dating a much broader range of metamorphic rocks. The methodology described here provides a valuable new tool for petrochronology and for directly constraining the timing of garnet growth, prograde metamorphism, and deep crustal processes. Garnet U-Pb geochronology can be used together with other conventional accessory mineral geochronometers but may be particularly powerful in geological settings where such chronometers are absent, scarce, or unsuitable.

Formatted: Superscript

Formatted: Superscript

Formatted: Superscript

Data availability

The data presented in this manuscript are available in the supplementary material.

Author contributions

AB conceptualised the study, obtained funding and carried out the formal analyses. Data curation, validation, and writing were done by all the authors through a continuous discussion process.

Competing interests

The authors declare that they have no conflict of interest.

Acknowledgements

We would like to thank Drs. Sonja Aulbach, Jose Ignacio Gil Ibarguchi, Qiao Shu and Robert Anczkiewicz for sharing the samples analysed in this study. The help of Linda Marko and Alex Schmidt with the day-to-day operation of the instruments makes everything easier. We also sincerely thank one anonymous reviewer, Dr. Ariela Mazoz and Dr. Martin Hugo Senger for their constructive and insightful reviews, which significantly improved the manuscript. Finally, we thank associate editor Dr. Brenhin Keller and handling editor Prof. Dr. Klaus Mezger for their careful handling of the review process.

Financial support

This work has been supported by the Deutsche Forschungsgemeinschaft (DFG) project number 521366037, granted to AB. FIERCE is financially supported by the Deutsche Forschungsgemeinschaft (DFG: INST 161/921-1 FUGG, INST 161/923-1 FUGG and INST 161/1073-1 FUGG), and received financial support from the Wilhelm and Else Heraeus Foundation, which is gratefully acknowledged. This is FIERCE contribution No. xxx.

References

Anczkiewicz, R. and Thirlwall, M. F.: Improving precision of Sm–Nd garnet dating by H_2SO_4 leaching: A simple solution to the phosphate inclusion problem, Spec. Publ. - Geol. Soc. Lond., 220, 83–91, https://doi.org/10.1144/GSL.SP.2003.220.01.05, 2003.

Anczkiewicz, R., Szczepański, J., Mazur, S., Storey, C., Crowley, Q., Villa, I. M., Thirlwall, M. F., and Jeffries, T. E.: Lu-Hf geochronology and trace element distribution in garnet: implications for uplift and exhumation of ultra-high pressure granulites in the Sudetes, SW Poland, Lithos, 95, 363–380, https://doi.org/10.1016/j.lithos.2006.09.001, 2007.

Arrowsmith, P.: Laser ablation of solids for elemental analysis by inductively coupled plasma mass spectrometry, Anal. Chem., 59, 1437–1444, https://doi.org/10.1021/ac00137a014,1987.

Aysal, N., Guillong, M., Bayanova, T., Fukuyama, M., Leonard, N., Yılmaz, İ., Varol, E., Tükel, F. Ş., Kadıoğlu, Y. K., Hanilçi, N., Uzun, F., and Kaygısız, E.: A New Natural Secondary Reference Material for Garnet U-Pb Dating by TIMS and LA-ICP-MS, Geostand. Geoanal. Res., 47, 297–310, https://doi.org/10.1111/ggr.12493, 2023.

Bartoli, O., Millonig, L. J., Carvalho, B. B., Marschall, H. R., and Gerdes, A.: The age of granulite-facies metamorphism in the Ivrea–Verbano Zone (NW Italy) determined through in situ U–Pb dating of garnet, J. Petrol., 65, egae083, https://doi.org/10.1093/petrology/egae083, 2024.

Baxter, E. F., Caddick, M. J., and Dragovic, B.: Garnet: A rock-forming mineral petrochronometer, Rev. Mineral. Geochem., 83, 469–533, https://doi.org/10.2138/rmg.2017.83.15, 2017.

Beno, C. J., Lackey, J. S., Schmitz, M. D., Bowman, J. R., Stearns, M. A., Bartley, J. M., and Fernandez, D. P.: Assessment of Natural Reference Materials for U–Pb Geochronology of Grossular-Andradite Garnet, Geostand. Geoanal. Res., 48, 909–925, https://doi.org/10.1111/ggr.12561, 2024.

Formatted: Subscript

Formatted: Subscript

Beranoaguirre, A., García de Madinabeitia, S., Sanchez-Lorda, M. E., Puelles, P., Ábalos, B., and Gil Ibarguchi, J. I.: U-Pb, Hf isotope and REE constraints on high-pressure acid migmatites from the Cabo Ortegal Complex (NW Spain): New evidence of short-duration metamorphism in a Variscan subduction channel, Lithos, 372–373, 105660, https://doi.org/10.1016/j.lithos.2020.105660, 2020.

Beranoaguirre, A., Vasiliev, I., and Gerdes, A.: In-situ LA-ICPMS U-Pb dating of Sulfates: Applicability of carbonate reference materials as matrix-matched standards, Geochronology, 4, 601–616, https://doi.org/10.5194/gchron-4-601-2022, 2022.

Caddick, M. J. and Kohn, M. J.: Garnet: Witness to the Evolution of Destructive Plate Boundaries Elements, 9, 427–432, https://doi.org/10.2113/gselements.9.6.427, 2013.

Cerva-Alves, T., Hartmann, L. A., Queiroga, G. N., Lana, C., Castro, M. P., Maciel, L. A. C., and Remus, M. V. D.: Metamorphic evolution of the juvenile Serrinha forearc basin in the southern Brasiliano Orogen, Precambrian Res., 365, 106394, https://doi.org/10.1016/j.precamres.2021.106394, 2021.

Cherniak, D. J.: Pb diffusion in rutile, Contrib. Mineral. Petrol., 139, 198–207, https://doi.org/10.1007/PL00007671, 2000.

Chew, D. M., Petrus, J. A., Kenny, G. G., and McEvoy, N.: Rapid high-resolution U–Pb LA-Q-ICPMS age mapping of zircon, J. Anal. At. Spectrom., 32, 262–276, https://doi.org/10.1039/C6JA00404K, 2017.

Chew, D. M., Petrus, J. A., Kenny, G. G., and McEvoy, N.: Rapid high-resolution U–Pb LA-Q-ICPMS age mapping of zircon, J. Anal. At. Spectrom., 32, 262–276, https://doi.org/10.1039/C6JA00404K, 2017.

Currie, L. A.: Nomenclature in evaluation of analytical methods including detection and quantification capabilities (IUPAC Recommendations 1995), Pure Appl. Chem., 67, 1699–1723, https://doi.org/10.1351/pac199567101699, 1995.

Dahl, P. S.: A crystal-chemical basis for Pb retention and fission-track annealing systematics in U-bearing minerals, with implications for geochronology, Earth Planet. Sci. Lett., 150, 277–290, https://doi.org/10.1016/S0012-821X(97)00108-8, 1997.

Dawson, J. B., Harley, S. L., Rudnick, R. L., and Ireland, T. R.: Equilibration and reaction in Archaean quartz-sapphirine granulite xenoliths from the Lace kimberlite pipe, South Africa, J. Metamorph. Geol., 15, 253–266, https://doi.org/10.1111/j.1525-1314.1997.00017.x, 1997.

Denèle, Y., Paquette, J. L., Olivier, P., and Barbey, P.: Permian granites in the Pyrenees: the Aya pluton (Basque Country), Terra Nova, 24, 105–113, https://doi.org/10.1111/j.1365-3121.2011.01043.x, 2012.

Deng, Y., Zhong, R., Li, D., Li, Y., and Cui, H.: Hunting the Datable Garnet using the LA-ICP-MS U-Pb Method: Predicting Garnet U Concentration, based on Major and Minor Elements, Acta Geol. Sin., 96, 2148–2157, https://doi.org/10.1111/1755-6724.14921, 2022.

Dodson, M. H.: Closure temperature in cooling geochronological and petrological systems, Contrib. Mineral. Petrol., 40, 259–274, https://doi.org/10.1007/BF00373790, 1973.

Duchêne, S., Blichert-Toft, J., Luais, B., Télouk, P., Lardeaux, J. M., and Albarède, F.: The Lu–Hf dating of garnets and the ages of the Alpine high-pressure metamorphism, Nature, 387, 586–589, https://doi.org/10.1038/42446, 1997.

Formatted: Spanish (Spain)

Formatted: Hyperlink, Spanish (Spain)

Field Code Changed

Flowers, R. M., Ketcham, R. A., Shuster, D. L., and Farley, K. A.: Apatite (U–Th)/He thermochronometry using a radiation damage accumulation and annealing model, Geochim. Cosmochim. Acta, 73, 2347–2365, https://doi.org/10.1016/j.gca.2009.01.015, 2009.

Fryer, B. J., Jackson, S. E., and Longerich, H. P.: The application of laser ablation microprobe-inductively coupled plasma-mass spectrometry (LAM-ICP-MS) to in situ U–Pb geochronology, Chem. Geol., 109, 1–8, https://doi.org/10.1016/0009-2541(93)90058-Q, 1993.

Gerdes, A. and Zeh, A.: Combined U–Pb and Hf isotope LA-(MC-)ICP-MS analyses of detrital zircons: comparison with SHRIMP and new constraints for the provenance and age of an Armorican metasediment in Central Germany, Earth Planet. Sci. Lett., 249, 47–61, https://doi.org/10.1016/j.epsl.2006.06.039, 2006.

Gerdes, A. and Zeh, A.: Zircon formation versus zircon alteration – new insights from combined U–Pb and Lu-Hf in-situ LA-ICPMS analyses, and consequences for the interpretation of Archean zircon from the Central Zone of the Limpopo Belt, Chem. Geol., 261, 230–243, https://doi.org/10.1016/j.chemgeo.2008.03.005, 2009.

Gray, A. L.: Solid sample introduction by laser ablation for inductively coupled plasma source mass spectrometry, Analyst, 110, 551–556, https://doi.org/10.1039/AN9851000551, 1985.

Harlov, D. E., Andersson, U. B., Förster, H.-J., Nyström, J. O., Dulski, P., and Broman, C.: Apatite–monazite relations in the Kiirunavaara magnetite–apatite ore, northern Sweden, Chem. Geol., 191, 47–72, https://doi.org/10.1016/S0009-2541(02)00148-1, 2002.

Harlov, D. E., Wirth, R., and Hetherington, C. J.: Fluid-mediated partial alteration of monazite: the role of dissolution–reprecipitation reactions, Contrib. Mineral. Petrol., 162, 329–348, https://doi.org/10.1007/s00410-010-0599-7, 2011.

Horstwood, M. S. A., Košler, J., Gehrels, G., Jackson, S. E., McLean, N. M., Paton, C., Pearson, N. J., Sircombe, K., Sylvester, P., Vermeesch, P., and Bowring, J. F.: Community-derived standards for LA-ICP-MS U-(Th-)Pb geochronology-Uncertainty propagation, age interpretation and data reporting, Geostand. Geoanal. Res., 40, 311–332, https://doi.org/10.1111/j.1751-908X.2016.00379.x, 2016.

Jackson, S. E., Pearson, N. J., Griffin, W. L., and Belousova, E. A.: The application of laser ablation-inductively coupled plasma-mass spectrometry to in situ U–Pb zircon geochronology, Chem. Geol., 211, 47–69, https://doi.org/10.1016/j.chemgeo.2004.06.017, 2004.

Jochum, K. P., Weis, U., Stoll, B., Kuzmin, D., Yang, Q., Raczek, I., Jacob, D. E., Stracke, A., Birbaum, K., Frick, D. A., Günther, D., and Enzweiler, J.: Determination of reference values for NIST SRM 610–617 glasses following ISO guidelines, Geostand. Geoanal. Res., 35, 97–429, https://doi.org/10.1111/j.1751-908X.2011.00120.x, 2011.

Kirkland, C. L., Ribeiro, B. V., and Slagstad, T.: In situ garnet Lu–Hf geochronology and constraints on metamorphism in the northernmost Norwegian Caledonides, J. Geol. Soc. Lond., https://doi.org/10.1144/jgs2024-193, 2025.

Kohn, M. J., Engi, M., and Lanari, P.: Petrochronology: Methods and applications, Rev. Mineral. Geochem., 83, https://doi.org/10.2138/rmg.2017.83.0, 2017.

Košler, J. and Sylvester, P. J.: Present trends and the future of zircon in geochronology: laser ablation ICP-MS, Rev. Mineral. Geochem., 53, 243–275, https://doi.org/10.2113/0530243, 2003.

Le Roex, A., Tinguely, C., and Gregoire, M.: Eclogite and Garnet Pyroxenite Xenoliths from Kimberlites Emplaced Along the Southern Margin of the Kaapvaal Craton, Southern Africa: Mantle or Lower Crustal Fragments?, J. Petrol., 61, egaa040, https://doi.org/10.1093/petrology/egaa040, 2020.

Li, D., Fu, Y., Hollings, P., Mitchell, R. H., Zurevinski, S., Kamo, S., Zhang, R., Zhang, Y., Liu, Q., Liao, J., Liang, Y., and Sun, X.: PL57 garnet as a new natural reference material for in situ U–Pb isotope analysis and its perspective for geological applications, Contrib. Mineral. Petrol., 177, 19, https://doi.org/10.1007/s00410-021-01884-4, 2022.

Ludwig, K. R.: User's Manual for Isoplot Version 3.75–4.15: a Geochronological Toolkit for Microsoft Excel, Berkeley Geochronological Center Special Publication, 5, 2012.

Machado, N. and Gauthier, G.: Determination of 207Pb/206Pb ages on zircon and monazite by laser-ablation ICP-MS and application to a study of sedimentary provenance and metamorphism in southeastern Brazil, Geochim. Cosmochim. Acta, 60, 5063–5073, https://doi.org/10.1016/S0016-7037(96)00287-6, 1996.

Madon, M., Gil-Ibarguchi, J. I., Via, J., and Girardeau, J.: Characterization and thermodynamic properties of andradite, Ca3Fe2Si3O12, Am. Mineral., 76, 1249–1260, 1991.

Manzotti, P., Millonig, L. J., Gerdes, A., Whitehouse, M. J., Jeon, H., Poujol, M., and Ballèvre, M.: Protolith age, and timing of burial and exhumation of the UHP Chasteiran Unit (Dora-Maira Massif, Western Alps), constrained by zircon, garnet and rutile petrochronology, Lithos, 496–497, 107951, https://doi.org/10.1016/j.lithos.2025.107951, 2025.

Mark, C., O'Sullivan, G., Glorie, A., Simpson, A., Andò, S., Barbarano, M., Stutenbecker, L., Daly, J. S., and Gilbert, S.: Detrital Garnet Geochronology by In Situ U-Pb and Lu-Hf Analysis: A Case Study From the European Alps, J. Geophys. Res. Earth Surf., 128, e2023JF007244, https://doi.org/10.1029/2023JF007244, 2023.

Martínez Catalán, J. R., Gómez Barreiro, J., Dias da Silva, I., Chichorro, M., López-Carmona, A., Castiñeiras, P., Abati, J., Andonaegui, P., Fernández-Suárez, J., González Cuadra, P., and Benítez-Pérez, J. M.: Variscan Suture Zone and Suspect Terranes in the NW Iberian Massif: allochthonous Complexes of the Galicia-Trás os Montes Zone (NW Iberia), in: The Geology of Iberia: A Geodynamic Approach, Volume 2: The Variscan Cycle, Springer, 99–130, https://doi.org/10.1007/978-3-030-10519-8_4, 2019.

McDougall, I. and Harrison, T. M.: Geochronology and Thermochronology by the 40Ar/39Ar Method, 2nd Edn., Oxford University Press, New York, 269 pp., ISBN 978-0195109207, 1999.

Millonig, L. J., Albert, R., Gerdes, A., Avigad, D., and Dietsch, C.: Exploring laser ablation U-Pb dating of regional metamorphic garnet - The Straits Schist, Connecticut, USA, Earth Planet. Sci. Lett., 552, 116589, https://doi.org/10.1016/j.epsl.2020.116589, 2020.

Münker, C., Weyer, S., Scherer, E. E., and Mezger, K.: Separation of high field strength elements (Nb, Ta, Zr, Hf) and Lu from rock samples for MC-ICPMS measurements, Geochem. Geophys. Geosyst., 2, 1088, https://doi.org/10.1029/2001GC000183, 2001.

Opendak, M. and Wildenhain, P.: On the analysis of the decay of a small number of radioactive atoms in radiochemical solar neutrino experiments, Nucl. Instrum. Methods Phys. Res. A, 345, 570–575, https://doi.org/10.1016/0168-9002(94)90517-7, 1994.

O'Sullivan, G. J., Hoare, B. C., Mark, C., Drakou, F., and Tomlinson, E. L.: Uranium–lead geochronology applied to pyrope garnet with very low concentrations of uranium, Geol. Mag., 160, 1010–1019, https://doi.org/10.1017/S0016756823000122, 2023.

Peillod, A., Patten, C. G. C., Drüppel, K., Beranoaguirre, A., Zeh, A., Gudelius, D., Hector, S., Majka, J., Kleine, B. I., Karlson, A., Gerdes, A., and Kolb, J.: Disruption of a high-pressure unit during exhumation: example of the Cycladic Blueschist Unit (Thera, Ios and Naxos islands, Greece), J. Metamorph. Geol., 42, 225–255, https://doi.org/10.1111/jmg.12753, 2024.

Pettke, T., Oberli, F., Audétat, A., Guillong, M., Simon, A. C., Hanley, J. J., and Klemm, L. M.: Recent developments in element concentration and isotope ratio analysis of individual fluid inclusions by laser ablation single and multiple collector ICP-MS, Ore Geol. Rev., 44, 10–38, https://doi.org/10.1016/j.oregeorev.2011.11.001, 2012.

Piccione, G., Rasbury, E. T., Elliott, B. A., Kyle, J. R., Jaret, S. J., Acerbo, A. S., Lanzirotti, A., Northrup, P., Wooton, K., and Parrish, R. R.: Vein fluorite U-Pb dating demonstrates post-6.2 Ma rare-earth element mobilization associated with Rio Grande rifting, Geosphere, 15, 1958–1972, https://doi.org/10.1130/GES02139.1, 2019.

Putnis, A.: Mineral replacement reactions, Rev. Mineral. Geochem., 70, 87–124, https://doi.org/10.2138/rmg.2009.70.3, 2009.

Reinhardt, N., Gerdes, A., Beranoaguirre, A., Frenzel, M., Meinert, L. D., Gutzmer, J., and Burisch, M.: Timing of magmatic-hydrothermal activity in the Variscan belt - LA-ICP-MS U-Pb geochronology of skarn-related garnet from the Schwarzenberg district, Erzgebirge, Mineral. Deposita, 57, 1071–1087, https://doi.org/10.1007/s00126-021-01084-x, 2022.

Reiners, P. W., Ehlers, T. A., and Zeitler, P. K.: Past, present, and future of thermochronology, Rev. Mineral. Geochem., 58, 1–18, https://doi.org/10.2138/rmg.2005.58.1, 2005.

Richter, S., Konegger-Kappel, S., Boulyga, S. F., Stadelmann, G., Koepf, A., and Siegmund, H.: Linearity testing and dead-time determination for MC-ICP-MS ion counters using the IRMM-072 series of uranium isotope reference materials, J. Anal. At. Spectrom., 31, 1647–1657, https://doi.org/10.1039/C6JA00203J, 2016.

Ring, U. and Gerdes, A.: Kinematics of the Alpenrhein-Bodensee graben system in the Central Alps: Oligocene/Miocene transtension due to formation of the Western Alps arc, Tectonics, 35, 1367–1391, https://doi.org/10.1002/2015TC004085, 2016.

Roberts, N. M. W. and Walker, R. J.: U–Pb geochronology of calcite-mineralized faults: absolute timing of rift-related fault events on the northeast Atlantic margin, Geology, 44, 531–534, https://doi.org/10.1130/G37868.1, 2016.

Rodriguez, J., Gil Ibarguchi, J. I., and Paquette, J. L.: Variscan synchronous magmatism across the Iberian Massif: new U-Pb ages in granitoids from the Fisterra area (A Coruña, Spain), XV Semana – VI Congresso Ibérico de Geoquímica, 2007.

Rubatto, D.: Zircon trace element geochemistry: Partitioning with garnet and the link between U–Pb ages and metamorphism, Chem. Geol., 184, 123–138, https://doi.org/10.1016/S0009-2541(01)00355-2, 2002.

Formatted: Font: Not Bold

Formatted: Font: Not Italic

Formatted: Font: Not Bold

Rubatto, D.: Zircon: the metamorphic mineral, Rev. Mineral. Geochem., 83, 261–295, https://doi.org/10.2138/rmg.2017.83.9, 2017.

Salnikova, E. B., Chakhmouradian, A. R., Stifeeva, M. V., Reguir, E. P., Kotov, A. B., Gritsenko, Y. D., and Nikiforov, A. V.: Calcic garnets as a geochronological and petrogenetic tool applicable to a wide variety of rocks, Lithos, 338–339, 141–154, https://doi.org/10.1016/j.lithos.2019.03.032, 2019.

Schaltegger, U., Schmitt, A. K., and Horstwood, M. S. A.: U-Th-Pb zircon geochronology by ID-TIMS, SIMS, and laser ablation ICP-MS: Recipes, interpretations, and opportunities, Chem. Geol., 402, 89–110, https://doi.org/10.1016/j.chemgeo.2015.02.028, 2015.

Schannor, M., Lana, C., Nicoli, G., Cutts, K., Buick, I., Gerdes, A., and Hecht, L.: Reconstructing the metamorphic evolution of the Araçuaí orogeny (SE Brazil) using in situ U–Pb garnet dating and P–T modelling, J. Metamorph. Geol., 39, 1145–1171, https://doi.org/10.1111/jmg.12605, 2021.

Schmitz, M. D. and Bowring, S. A.: Constraints on the thermal evolution of continental lithosphere from U–Pb accessory mineral thermochronology of lower crustal xenoliths, southern Africa, Contrib. Mineral. Petrol., 144, 592–618, https://doi.org/10.1007/s00410-002-0419-9, 2003.

Seman, S., Stockli, D. F., and McLean, N. M.: U-Pb geochronology of grossular-andradite garnet, Chem. Geol., 460, 106–116, https://doi.org/10.1016/j.chemgeo.2017.04.020, 2017.

Shu, Q., Beranoaguirre, A., Albert, R., Millonig, L. J., Walters, J. B., Marschall, H. R., Gerdes, A., Hoefer, H. E., Hezel, D., and Brey, G. P.: Multi-stage ultrahigh temperature metamorphism in the lower crust of the Kaapvaal craton recorded by U–Pb ages of garnet, Contrib. Mineral. Petrol., 179, 49, https://doi.org/10.1007/s00410-024-02121-4, 2024.

Simpson, A., Gilbert, S., Tamblyn, R., Hand, M., Spandler, C., Gillespie, J., Nixon, A., and Glorie, S.: In situ Lu–Hf geochronology of garnet, apatite and xenotime by LA-ICP-MS/MS, Chem. Geol., 577, 120299, https://doi.org/10.1016/j.chemgeo.2021.120299, 2021.

Spear, F. S. and Parrish, R. R.: Petrology and cooling rates of the Valhalla Complex, British Columbia, Canada, J. Petrol., 37, 733–765, https://doi.org/10.1093/petrology/37.4.733, 1996.

Stifeeva, M. V., Salnikova, E. B., Samsonov, A. V., Kotov, A. B., and Gritsenko, Y. D.: U-Pb geochronology of garnet from Daschkesan skarn deposit (Lesser Caucasus), Dokl. Earth Sci., 487, 953–956, https://doi.org/10.1134/S1028334X19080178, 2019.

Stifeeva, M., Salnikova, E., Adamskaya, E., Millonig, L. J., Ivanov, A., Mottram, C., Kovach, V., Kotov, A., Bryanskiy, N., Karimov, A., Gladkochub, E., Peytcheva, I., Gerdes, A., Bowie, S., and Gritsenko, J.: Kovdor-GRT – A New Natural Reference Material for Garnet U-Pb Dating, Geostand. Geoanal. Res., https://doi.org/10.1111/ggr.70040, 2026.

Sylvester, P. J. and Jackson, S. E.: A Brief History of Laser Ablation Inductively Coupled Plasma Mass Spectrometry (LA–ICP–MS), Elements, 12, 307–310, https://doi.org/10.2113/gselements.12.5.307, 2016.

Szczepański, J. and Ilnicki, S.: From Cadomian arc to Ordovician passive margin: geochemical records preserved in metasedimentary successions of the Orlica-Snieznik Dome in SW Poland, Int. J. Earth Sci., 103, 627–647, https://doi.org/10.1007/s00531-013-0993-2, 2014.

Tamblyn, R., Hand, M., Simpson, A., Gilbert, S., Wade, B., and Glorie, S.: In situ laser ablation Lu–Hf geochronology of garnet across the Western Gneiss Region: campaign-style dating of metamorphism, J. Geol. Soc. Lond., 179, jgs2021-094, https://doi.org/10.1144/jgs2021-094, 2022.

Tera, F. and Wasserburg, G. J.: U-Th-Pb systematics in three Apollo 14 basalts and the problem of initial Pb in lunar rocks, Earth Planet. Sci. Lett., 14, 281–304, https://doi.org/10.1016/0012-821X(72)90128-8, 1972.

Walczak, K., Anczkiewicz, R., Szczepański, J., Rubatto, D., and Košler, J.: Combined garnet and zircon geochronology of the ultra-high temperature metamorphism: Constraints on the rise of the Orlica-Śnieżnik Dome, NE Bohemian Massif, SW Poland, Lithos, 292–293, 388–400, https://doi.org/10.1016/j.lithos.2017.09.013, 2017.

Walters, J. B., Garber, J. M., Beranoaguirre, A., Millonig, L. J., Gerdes, A., Grützner, T., and Marschall, H. R.: Zircon micro-inclusions as an obstacle for in situ garnet U-Pb geochronology: An example from the As Sifah eclogite locality, Oman, Geochronology, 7, 309–333, https://doi.org/10.5194/gchron-7-309-2025, 2025.

Willigers, B. J. A., Baker, J. A., Krogstad, E. J., and Peate, D. W.: Precise and accurate in situ Pb-Pb dating of apatite, monazite, and sphene by laser ablation multiple-collector ICP-MS, Geochim. Cosmochim. Acta, 6, 1051–1066, https://doi.org/10.1016/S0016-7037(01)00838-9, 2002.

Yang, Y., Wu, S., Wang, H., Kamo, S. L., Ma, Q., Liang, T., Xu, L., Xie, L., Huang, C., Wan, B., Yang, J., and Wu, F.: Three new natural secondary reference materials for in situ andradite U–Pb geochronology, J. Anal. At. Spectrom., 40, 326–337, https://doi.org/10.1039/D4JA00290C, 2025.

Zack, T. and Kooijman, E.: Petrology and geochronology of rutile, Rev. Mineral. Geochem., 83, 443–467, https://doi.org/10.2138/rmg.2017.83.14, 2017.